Resonant x-ray diffraction study of the charge ordering in magnetite

2005 J. Phys.: Condens. Matter 17 7633

(http://iopscience.iop.org/0953-8984/17/48/015)

INSTITUTE OF PHYSICS PUBLISHING JOURNAL OF PHYSICS: CONDENSED MATTER

J. Phys.: Condens. Matter **17** (2005) 7633–7642 doi:10.1088/0953-8984/17/48/015

Resonant x-ray diffraction study of the charge ordering in magnetite

Richard J Goff[1,2], Jon P Wright[3], J Paul Attfield[1] and Paolo G Radaelli[4]

[1] Centre for Science at Extreme Conditions, University of Edinburgh, Erskine Williamson Building, King's Buildings, Mayfield Road, Edinburgh EH9 3JZ, UK
[2] Department of Chemistry, University of Cambridge, Lensfield Road, Cambridge CB2 1EW, UK
[3] European Synchrotron Radiation Facility, BP-220, 38043 Grenoble, France
[4] ISIS Facility, Rutherford Appleton Laboratories, Chilton, Didcot OX11 0QX, UK

Received 12 July 2005, in final form 25 October 2005
Published 11 November 2005
Online at stacks.iop.org/JPhysCM/17/7633

Abstract

Powder x-ray diffraction patterns of magnetite (Fe_3O_4) have been recorded at 90 K, below the Verwey transition, at three wavelengths in the pre- to mid-edge region of the 7.1 keV Fe K absorption. Simultaneous fitting of these profiles has been used to refine the anomalous scattering coefficients for the octahedral B site iron atoms. The refined values give direct evidence for a significant degree (46%) of Fe^{2+}/Fe^{3+} charge ordering in magnetite, and provide new constraints on the number of possible charge ordered models.

1. Introduction

Charge ordering below the 122 K Verwey transition in magnetite, Fe_3O_4, has been investigated for over 60 years but remains controversial [1–3]. The first reported evidence of the transition was a heat capacity anomaly [4], and Verwey [5] discovered that magnetite undergoes a first order transition at 120 K, at which the resistivity increases by two orders of magnitude. The structure distorts from cubic symmetry and an orthorhombic model, in which the Fe^{2+} and Fe^{3+} ions were charge ordered over the octahedral B sites of the spinel arrangement, was proposed. This model was thought to have been confirmed by single-crystal neutron diffraction [6] but the experiment was later shown to be flawed due to multiple scattering [7]. The observation of further superstructure peaks [8], which could be indexed as $(h, k, l+1/2)$ on the cubic unit cell and were not predicted by the Verwey model, showed that the symmetry must be monoclinic. Detailed neutron diffraction studies [9] proposed Cc symmetry with a $\sqrt{2}a \times \sqrt{2}a \times 2a$ supercell. Refinements were carried out on an almost fully de-twinned single crystal using an $a/\sqrt{2} \times a/\sqrt{2} \times 2a$ subcell with $Pmca$ or $Pmc2_1$ orthorhombic pseudosymmetries, but no charge ordered arrangement was identified.

Mössbauer spectroscopy [10, 11] has identified five different Fe environments, which have been interpreted as tetrahedral Fe^{3+}, two different octahedral Fe^{3+} sites, and two different octahedral Fe^{2} sites. ^{57}Fe NMR [12, 13] has identified the 16 B site signals expected from

the Cc supercell. Experiments on nanoparticles showed that particles with dimensions of a few unit cells can support long range charge order [14]. Other experiments on both oxidized and unoxidized magnetite nanoparticles show that the charge ordering enhances the lattice distortion rather than being the result of the lattice distortion [15].

Direct structural observation of charge ordering [16] was recently obtained from a combined x-ray and neutron powder diffraction refinement of the $P2/c$ subcell structure with $Pmca$ symmetry constraints as used before [9]. Significant differences in the octahedral Fe–O distances were analysed using bond valence sums and a family of possible charge ordered models was proposed. These do not satisfy the criterion of Anderson [17] that each tetrahedral group of four B sites should contain two electrons (i.e. $2Fe^{2+}$ and $2Fe^{3+}$).

Ab initio electronic structure calculations using coordinates from the above study have predicted a $[001]_c$ charge density wave with a minor $[00\frac{1}{2}]_c$ modulation [18] with a charge disproportionation of 23%. Other calculations have predicted a charge order of 32% [19] and 20% [20, 21]. It has also been suggested that the structural distortions observed cause the charge disproportionation [22], but a complicated charge ordered arrangement was not ruled out. Scanning tunnelling microscopy has seen alternation of Fe^{2+} dimers and Fe^{3+} dimers along chains on the (100) surface [23]. X-ray emission spectroscopy experiments have supported charge order [24], itinerant electrons below T_V [25] and strong electron–lattice coupling [26].

Resonant x-ray diffraction, making use of the enhanced anomalous scattering terms close to the 7.13 keV Fe K edge, should be sensitive to Fe^{2+}/Fe^{3+} order below the Verwey transition. However, DAFS (diffraction anomalous fine structure) experiments have been inconclusive, with both charge ordered [27] and itinerant electron models [28] proposed. DAFS experiments draw information from the detailed energy variation of a few structure factors through the Fe K edge. In this study we have taken an alternative approach by analysing a complete set of powder diffraction intensities at a few on-edge wavelengths. Rietveld profile fitting is used to refine values of the anomalous dispersion corrections, which differ significantly because of the shift of the absorption edge to higher energies with increasing charge state. This approach has previously been used to observe Eu^{2+}/Eu^{3+} order in Eu_3O_4 [29], Ga^{+}/Ga^{3+} order in $GaCl_2$ [30] and Fe^{2+}/Fe^{3+} order in Fe_2PO_5 [31].

2. Experiment

The polycrystalline Fe_3O_4 sample was the same as in previous experiments [16]. X-ray diffraction data were recorded on instrument ID31 at ESRF, Grenoble. Half-annular geometry was used to minimize absorption. A monochromator scan was used to measure the Fe K edge fluorescence spectrum (figure 1). High-resolution x-ray diffraction patterns were then recorded up to $2\theta = 150°$ for eight hours each at three selected energies (shown in figure 1). $\lambda_1 = 1.745\,11$ Å (7112.7 eV) is at a non-absorbing pre-edge energy, $\lambda_2 = 1.742\,81$ Å (7122.1 eV) is at the pre-edge absorption from Fe^{3+} on the tetrahedral A-sites [32], and $\lambda_3 = 1.741\,38$ Å (7128.0 eV) is at a mid-edge energy. Changes in diffraction intensity due to the energy variation of resonant scattering are clearly seen, particularly in the λ_3 pattern (figure 2).

The three diffraction patterns were fitted simultaneously using the GSAS software [33] package. The previously reported model was used [16] and the coordinates were not varied. The peak shapes were fitted as in the previous refinement [16] and were constrained to be the same for the three patterns. Preferred crystallite orientation was observed because of the half-annular sample geometry and this was fitted using the March model with a unique $[\bar{1}04]$ axis, which corresponds to the cubic [111] direction. Sample absorption was fitted using the Pitschke model for surface roughness in the GSAS software package [33]. Two temperature factors (for

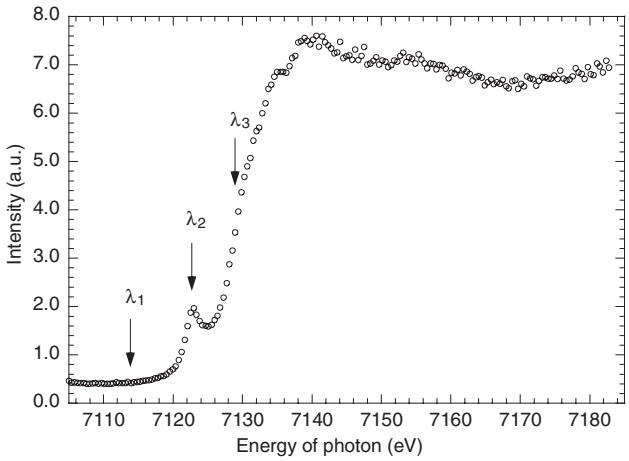

Figure 1. The Fe K absorption edge of polycrystalline Fe_3O_4 at 90 K. The three wavelengths used in the diffraction experiments (λ_1, λ_2, λ_3) are indicated.

Fe and O atoms) were also refined, to make a further correction for absorption effects. The real (f') and imaginary (f'') anomalous dispersion corrections for Fe were refined according to the models described below. Only f' values were refined in the pre-edge λ_1 diffraction pattern and f'' was fixed at the value of 0.47 electrons/atom calculated from the program fprime within the GSAS software package [33]. λ_2 coincides with the pre-edge absorption of the tetrahedral Fe sites, so f'' was refined for the A sites, while f'' for the B sites was fixed at a value of 0.84 e/atom, estimated from the increase in the absorption between λ_1 and λ_2 (figure 1). f' values were also refined. Both f' and f'' were refined against the mid-edge λ_3 diffraction pattern.

3. Resonant diffraction analysis

Initial refinements showed that the overall profile fitting residuals are rather insensitive to various f' and f'' constraints between the Fe sites. This is not surprising because information about atomic displacements and B site charge differences is contained mainly in the weak superstructure peaks, whereas the profile R-factors are dominated by slight imperfections in the peak shape and background fitting functions, and small systematic errors (e.g. extinction) in the very intense fundamental reflection intensities. However, the intensity residuals for classes of ($h\,k\,l$) reflections that are sensitive to charge ordering do show significant differences between models, and we use this approach (which is typically used to analyse weak superstructures from single-crystal x-ray diffraction data) as described later.

Refinement of the anomalous scattering coefficients was initially carried out using the f' and f'' constraints described above, and with coefficients also constrained by $Pmca$ space group symmetry ('$Pmca$-split' model). The anomalous terms for the four B sites were refined independently. The two A sites were initially refined separately as well, but their anomalous terms were found to be the same within error so they were constrained to be equal thereafter in this and other models described below. The greatest dispersion between refined resonant terms was, as expected, found for the mid-edge λ_3 data. The values for the B sites in table 1 show a small dispersion in f' (0.4 e/atom; 4% of the average B site f'), but a much larger dispersion for the imaginary f'' terms (0.7 e/atom; 42% of the average f'') is found at this energy. Both

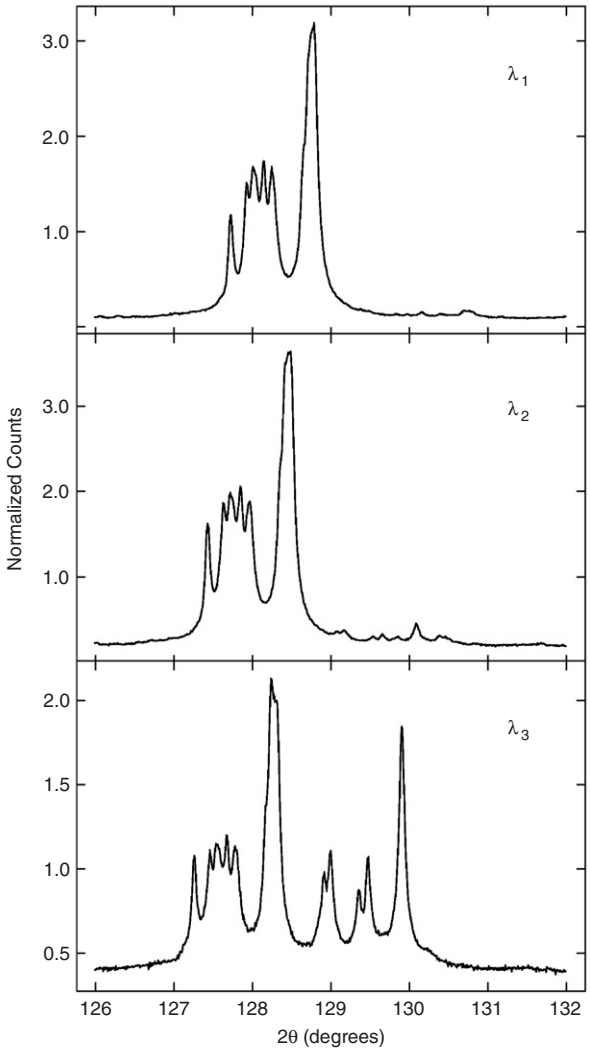

Figure 2. Part of the diffraction patterns of Fe_3O_4 at 90 K for the three wavelengths λ_1, λ_2, and λ_3 showing the sensitivity of the diffraction intensities to changes in resonant scattering at the Fe K edge. The first family of peaks (at $2\theta = 127.0°$–$128.7°$ for λ_3) are the split cubic (751), (555) peak, and the second set ($2\theta = 128.7°$–$130.5°$) derives from the cubic (662) peak.

sets of values correlate with the formal Fe site valences previously deduced from the Fe–O distances [16], with larger (more negative) f' and (more positive) f'' for the lower valence sites due to the shift of absorption edge to higher energies with increasing Fe valence. The difference between the f'' values for the high valence (B2 and B3) and low valence (B1 and B4) sites is particularly clear and corroborates the valence distribution proposed previously [16]. The A site values do not follow the same valence trend as the B sites because the shape of the absorption edge for the tetrahedral A sites is likely to be quite different from that for the octahedral B sites, as shown by the pre-edge A site absorption maximum.

In the previous structural analysis [16], a monoclinic $P2/c$ symmetry subcell was used with atomic positions further constrained by orthorhombic $Pmca$ symmetry operations. This creates four inequivalent B sites (B1–B4), each of which averages over four more sites in

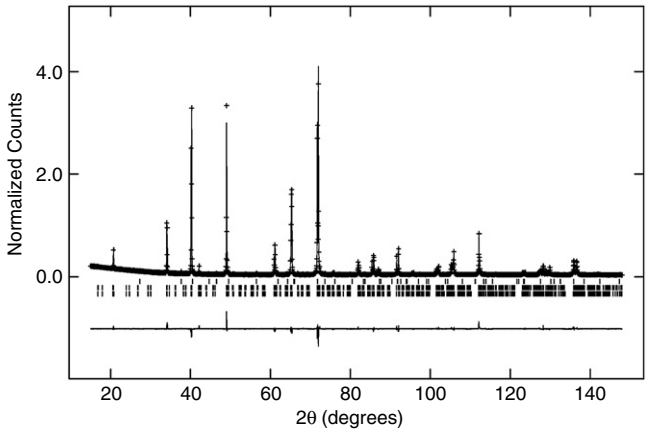

Figure 3. The observed, calculated and difference plots for the fit of the $P2/c$-split model to the λ_3 diffraction pattern (1.741 38 Å) of Fe_3O_4 at 90 K.

Table 1. Formal valences (V) and values of f' and f'' for λ_3 (1.741 38 Å) for the $Pmca$-split refinement model for Fe_3O_4 at 90 K.

	V	$f'(\lambda_3)$ (e/atom)	$f''(\lambda_3)$ (e/atom)
A[a]	3	−9.64(3)	2.44(4)
B1	2.25	−9.77(6)	2.12(9)
B2	2.75	−9.40(6)	1.39(9)
B3	2.75	−9.54(9)	1.45(12)
B4	2.25	−9.51(8)	2.13(11)

[a] In $Pmca$, there are two inequivalent A site cations, but these are constrained to have equal scattering factors.

the 'true' Cc supercell (which contains 16 unique B sites). The octahedral sites determined previously [16] and their descent in symmetry from $Pmca$ to $P2/c$ are shown in table 2. If the $Pmca$ constraints are removed then the two high symmetry B sites (B1 and B2) each split into two distinct twofold sites (B1a and B1b; B2a and B2b) in monoclinic $P2/c$ symmetry, whereas the B3 and B4 sites remain equivalent. This '$P2/c$-split' model was fitted to the three data sets, with the anomalous terms for the six independent B sites refined independently. Residuals are shown in table 3, and the refined resonant coefficients at all three wavelengths are given in table 4. The observed, calculated and difference plots for the fit to the mid-edge λ_3 diffraction pattern are shown in figure 3.

Although f' and f'' are treated as independent variables in the above refinements, these quantities are linked physically through Kramers–Kronig integrals. However, useful refinement constraints between the variables cannot be made without knowledge of the energy variations of the individual site absorption spectra. The average refined f' and f'' values at each energy may be used as a check of self-consistency. The f'' averages in table 4 scale with the edge spectrum in figure 1 and the average (and individual site) f' and f'' values are comparable to those derived from x-ray absorption studies of magnetite [32, 34], showing that the refined values are physically realistic.

In our $Pmca$-constrained valence analysis, the B1 site averages over ($3Fe^{2+} + Fe^{3+}$) formal states, so lowering the symmetry to $P2/c$ is expected to split B1 into subsites that have a

Table 2. Octahedral (B) sites in the low temperature $a/\sqrt{2} \times a/\sqrt{2} \times 2a$ subcell of magnetite in the $Pmca$ and $P2/c$ symmetry descriptions.

$Pmca$			$P2/c$		
Site		(x, y, z)	Site		(x, y, z)
B1	4b	(0, 0.5, 0)	B1a	2c	(0, 0.5, 0)
			B1b	2b	(0.5, 0.5, 0)
B2	4c	(0, 0.010, 0.25)	B2a	2e	(0, 0.010, 0.25)
			B2b	2f	(0.5, 0.010, 0.25)
B3	4d	(0.25, 0.266, 0.380)	B3	4g	(0.25, 0.266, 0.380)
B4	4d	(0.25, 0.752, 0.377)	B4	4g	(0.25, 0.752, 0.377)

Table 3. The fitting parameters for the average and $P2/c$ split models for Fe_3O_4 at 90 K. The fitting of $(h\ k\ l/2)$ reflections are also given for λ_3.

	Average model	$P2/c$ split model
Overall R_{wp}	0.0762	0.0760
Overall R_{F^2}	0.0470	0.0466
$\lambda_3 R_{F^2}$ $(o\ o\ o)$	0.4096	0.2942
$\lambda_3 R_{F^2}$ $(o\ e\ e)$	0.3915	0.3716
$\lambda_3 R_{F^2}$ $(o\ o\ e)$	0.0646	0.0623
$\lambda_3 R_{F^2}$ $(o\ e\ o)$	0.0410	0.0410

Table 4. Formal valences (V) and values of f' and f'' for the three wavelengths λ_1, λ_2, and λ_3 (1.745 11, 1.742 81, and 1.741 38 Å, respectively) for the $P2/c$-split model for Fe_3O_4 at 90 K. The weighted average f' and f'' for Fe are also given. Values of f'' shown without an e.s.d. (estimated standard deviation) were not refined.

	V	$f'(\lambda_1)$ (e/atom)	$f''(\lambda_1)$ (e/atom)	$f'(\lambda_2)$ (e/atom)	$f''(\lambda_2)$ (e/atom)	$f'(\lambda_3)$ (e/atom)	$f''(\lambda_3)$ (e/atom)
A[a]	3.0	−7.20(3)	0.47	−7.87(3)	0.97(6)	−9.61(3)	2.50(4)
B1a	2.5	−7.50(5)	0.47	−8.31(5)	0.84	−9.53(9)	1.68(12)
B1b	2.0	−7.71(6)	0.47	−8.52(5)	0.84	−9.87(11)	2.50(16)
B2a	3.0	−7.28(5)	0.47	−7.89(5)	0.84	−9.08(11)	0.88(16)
B2b	2.5	−7.27(5)	0.47	−8.13(5)	0.84	−9.63(9)	1.98(13)
B3	2.75	−7.33(5)	0.47	−8.15(5)	0.84	−9.58(10)	1.47(14)
B4	2.25	−7.27(5)	0.47	−8.12(5)	0.84	−9.47(9)	2.21(13)
Average		−7.31(4)	0.47	−8.07(4)	0.88(2)	−9.55(8)	2.03(11)

[a] In $P2/c$, there are two inequivalent A site cations, but these are constrained to have equal scattering factors.

formal average valence of 2.0 ($2Fe^{2+}$) and 2.5 ($Fe^{2+} + Fe^{3+}$). Similarly, B2 ($3Fe^{3+} + Fe^{2+}$) states should split into subsites with average valences of 2.5 and 3.0. The expected formal Fe valences for the $P2/c$-split model are shown in table 4. At resonant energies where f' and f'' vary with Fe valence state, the reflections that are sensitive to the split B1 and B2 sites are $(o\ k\ e)$ (o, e refer to odd, even numbers throughout), indexed on the $a/\sqrt{2} \times a/\sqrt{2} \times 2a$ cell, and these can be split into two groups according to whether $h + k + l/2$ is odd or even. The structure factors for these two groups are

$$F_{hkl} \approx \pm 2[(f_{1a} - f_{1b}) + (f_{2a} - f_{2b})] + G_{hkl} \qquad h + k + l/2 \text{ is odd}$$
$$F_{hkl} \approx \pm 2[(f_{1a} - f_{1b}) - (f_{2a} - f_{2b})] + G_{hkl} \qquad h + k + l/2 \text{ is even}$$

where f_{1a} is the scattering factor for site B1a, etc, and G_{hkl} is a weakly energy dependent

term. If the resonant contributions vary linearly with formal Fe valence, then the differences $(f_{1a} - f_{1b})$ and $(f_{2a} - f_{2b})$ will cancel in one of the above cases and reinforce to give a strong resonant term in the other, depending on the valence distribution over the split B1 and B2 sites.

Table 3 compares fitting residuals for the $P2/c$-split model with an 'Average' model, in which the anomalous terms for the B-sites were held equal, so the resonant differences in the above equations are fixed at zero. The odd $h + k + l/2$ reflections $(o\ o\ o)$ and $(o\ e\ e)$ are systematically absent in the high temperature cubic magnetite structure, and so these superstructure reflections are very weak in x-ray scattering and the R_{F^2} residuals are high, but show a significant reduction in the $P2/c$-spilt model compared to the Average fit (table 3). This shows that the $(f_{1a} - f_{1b})$ and $(f_{2a} - f_{2b})$ differences have the same sign. The even $h+k+l/2$ reflections $(o\ o\ e)$ and $(o\ e\ o)$ are stronger (they are allowed in cubic symmetry) but show no significant difference between Average and $P2/c$-spilt refinements, as the $(f_{1a} - f_{1b})$ and $(f_{2a} - f_{2b})$ differences essentially cancel out.

The real anomalous scattering coefficient f' is negative and goes through a minimum at the Fe K edge, whereas f'' is proportional to absorption and so is positive and increases at the edge. The Fe^{3+} absorption edge is shifted by approximately 5 eV to higher energy relative to that of Fe^{2+} [34], so at pre- to mid-edge energies f' is expected to become more positive with increasing Fe valence, whereas f'' becomes less positive (assuming the edge does not change shape significantly with octahedral site valence). The plots of refined values of f' and f'' for the $P2/c$-split model from table 4 against formal Fe valence in figure 4 are consistent with these predictions. As for the $Pmca$-split refinement, the variations of f' are small at the pre-edge wavelengths λ_1 and λ_2, and even at the mid-edge energy λ_3. The f' values for the B3, B4, and the average valence B1a and B2b sites are similar; however, f' for the low valence B1b and high valence B2a sites show the expected trend. f'' is more sensitive to valence state at the λ_3 energy and the six values show a clear correlation with formal Fe site valence.

These results demonstrate that small differences in Fe K edge resonant scattering are consistent with charge ordering in magnetite below the Verwey transition. The difference of 0.79 e/atom between the $f'(\lambda_3)$ values for B1b (formal valence 2) and B2a (formal valence 3) is 46% of that between the corresponding $f'(Fe^{2+}) = -9.74$ e/atom and $f'(Fe^{3+}) = -8.04$ e/atom values for Fe_2PO_5 [31] which we take as an estimate for a fully charge separated material (as there is no pseudosymmetry between the Fe^{2+} and Fe^{3+} sites). This shows that the charge separation in the full Cc monoclinic $\sqrt{2}a \times \sqrt{2}a \times 2a$ structure of magnetite is 46% of the ideal value, which is averaged to 23% in the $Pmca$-constrained $a/\sqrt{2} \times a/\sqrt{2} \times 2a$ subcell. This is in excellent agreement with the 20% charge order based on the Fe–O distances in the latter refinement [16] and the 20–30% charge order from electronic structure calculations [18–21]. The splittings of the valences on the B1 and B2 sites directly corroborate the previous assumption that these were respectively averaging over $(3Fe^{2+} + Fe^{3+})$ and $(3Fe^{3+} + Fe^{2+})$ sites in the full low temperature superstructure.

4. Charge ordering models

The new information about the charge distribution over the split B1 and B2 sites in the $P2/c$ subcell reduces the number of charge ordered arrangements that are possible for the full $\sqrt{2}a \times \sqrt{2}a \times 2a$ supercell. There are 16 arrangements that are compatible with the valences determined and Cc symmetry [9]. These may be grouped into nine classes of charge ordering model according to the numbers N_T of unique $(Fe^{2+})_n(Fe^{3+})_{4-n}$ tetrahedra; n equals the number of electrons localized per tetrahedron. Table 5 confirms that none of the solutions satisfy the Anderson criterion [17], which requires all tetrahedra to have $n = 2$. Up to five-eighths of the tetrahedra can be Anderson-like, although this requires one tetrahedron to have

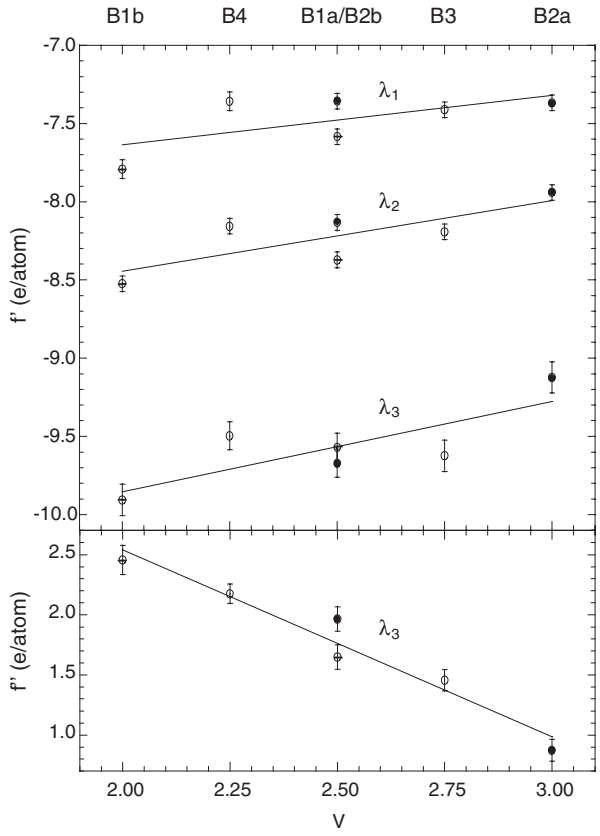

Figure 4. The $P2/c$-split values of f' and f'' (for the λ_3 diffraction pattern only) plotted as a function of the formal valences of the B-site Fe ions in Fe_3O_4 at 90 K. The symbols for the B1 subsites contain a horizontal line while the B2 subsite symbols are filled.

Table 5. The 16 possible charge ordering models in the full Cc cell of Fe_3O_4 grouped into nine classes according to the number $N_T(n)$ of symmetry inequivalent $(Fe^{2+})_n(Fe^{3+})_{4-n}$ tetrahedra.

	$N_T(n)$					
Class	0	1	2	3	4	Number of models
A		2	4	2		4
B		3	2	3		2
C	1	1	4	1	1	2
D	1	1	3	3		2
E		3	3	1	1	2
F	1		5	2		1
G		2	5		1	1
H	1	2	1	4		1
I		4	1	2	1	1

$n = 0$ or 4 (solutions F and G). The four class A models minimize Coulombic interactions through having four Anderson tetrahedra while the other four have $n = 1$ or 3.

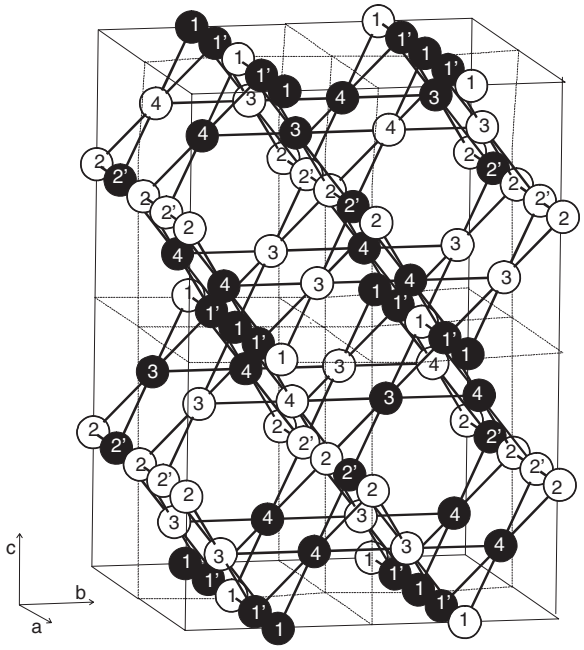

Figure 5. One of eight possible models for charge ordering on the B sites in the full $\sqrt{2}a \times \sqrt{2}a \times 2a$ Cc supercell of magnetite that is consistent with the valences from the $P2/c$-split model. The B sites are labelled, with B1a and B1b represented by 1 and 1′ etc. The dark/light circles represent Fe^{2+}/Fe^{3+}.

Figure 5 shows a plausible class A model. The total charge in each *ab*-plane layer defines a $[001]_c$ charge density wave. The layers have a checkerboard arrangement of Anderson and non-Anderson tetrahedra. Two layers of electron rich tetrahedra are followed by two layers of electron poor tetrahedra; the second is displaced by $a/4$ (equivalent to one Fe–Fe bond distance) relative to the first layer. These displacements produce the additional $[00\frac{1}{2}]_c$ charge modulation wave. The chains in the a-direction are consistent with 3:1 (or 1:3) ordering of Fe^{2+} and Fe^{3+} seen in x-ray diffuse scattering above T_V [35]. The alternation of Fe^{2+} dimers and Fe^{3+} dimers along chains in the b-direction at $z = 3/8, 7/8$ is consistent with the same dimers seen on the (001) surface by scanning tunnelling microscopy [23] and the dimers observed by NMR [13]. A $[00\frac{1}{2}]_c$ modulation was also observed in the positions of the 3:1 ordered chains (at $z = 0, 1/2$ and $z = 1/4, 3/4$), 1:1 ordered chains (at $z = 1/8, 5/8$) and dimers (at $z = 3/8, 7/8$). The presence of both $[001]_c$ and $[00\frac{1}{2}]_c$ modulations is consistent with both diffraction studies [16] and theoretical calculations [18].

5. Conclusions

Analysis of Fe K edge resonant x-ray diffraction data for magnetite below the Verwey transition has revealed scattering differences that are consistent with the previous published charge ordering based on the Fe–O distances. This provides direct evidence for charge ordering in magnetite. Refinement of B site anomalous scattering coefficients does not improve the overall profile fit, but significantly improves the fit to the very weak superstructure reflections that are sensitive to the differences between the split B1 and B2 sites. The refined f'' values show a clear correlation with formal Fe valence. The differences in f' and f'' between the

formal Fe^{2+} and Fe^{3+} states are small, in keeping with the reduced magnitude of real charge separation in symmetry-broken, charge ordered, transition metal oxides. The derived valences for the split B1 and B2 sites have provided new constraints on the charge ordering in the full *Cc* supercell of magnetite, leading to 16 possible models.

References

[1] Mott N F 1980 *Phil. Mag.* B **42** 327
[2] Walz F 2002 *J. Phys.: Condens. Matter* **14** 285
[3] Garcia J and Subias G 2004 *J. Phys.: Condens. Matter* **16** 145
[4] Parks G S and Kelley K K 1926 *J. Phys. Chem.* **30** 47
[5] Verwey E J W 1939 *Nature* **144** 327
Verwey E J W and Haayman P W 1941 *Physica* **9** 979
Verwey E J W, Haayman P W and Romeijan F C 1947 *J. Phys. Chem.* **15** 181
[6] Hamilton W C 1958 *Phys. Rev.* **110** 1050
[7] Shirane G, Chikazumi S, Akimitsu J, Chiba K, Matsui M and Fuji Y 1975 *J. Phys. Soc. Japan* **39** 949
[8] Samuelson E J, Bleeker E J, Dobrzynski L and Riste T J 1968 *Appl. Phys.* **39** 1114
[9] Iizumi M and Shirane G 1975 *Solid State Commun.* **17** 433
Iizumi M, Koetzle T F, Shirane G, Chikazumi S, Matsui M and Todo S 1982 *Acta Crystallogr.* B **38** 2121
[10] Berry F J, Skinner S and Thomas M F 1998 *J. Phys.: Condens. Matter* **10** 215
[11] Sorescu M, Diamandescu L, Brand R A and Tarabasanu-Mihaila D 2004 *Mater. Lett.* **58** 885
[12] Novak P, Stepankova H, Englich J, Kohout J and Braber V A M 2000 *Phys. Rev.* B **61** 1256
[13] Mizoguchi M 2001 *J. Phys. Soc. Japan* **70** 2333
[14] Poddar P, Fried T, Markovic G, Sharoni A, Katz D, Wizansky T and Millo O 2003 *Europhys. Lett.* **64** 98
[15] Wang J, Chen Q, Li X, Shi L, Peng Z and Zeng C 2004 *Chem. Phys. Lett.* **390** 55
[16] Wright J P, Attfield J P and Radaelli P G 2001 *Phys. Rev. Lett.* **87** 266401
Wright J P, Attfield J P and Radaelli P G 2002 *Phys. Rev.* B **66** 214422
[17] Anderson P W 1956 *Phys. Rev.* **15** 1008
[18] Leonov I, Yaresko A N, Antonov V N, Korotin M A and Anisimov V I 2004 *Phys. Rev. Lett.* **93** 146404
[19] Anisimov V I, Elfimov I S, Hamada N and Tekura K 1996 *Phys. Rev.* B **54** 4387
[20] Jeng H-T, Guo G Y and Huang D J 2004 *Phys. Rev. Lett.* **93** 156403
[21] Madsen G K H and Novak P 2004 *Preprint* cond-mat/0412560
[22] Szotek Z, Temmerman W M, Svane A, Petit L, Stocks G M and Winter H 2003 *Phys. Rev.* B **68** 054415
[23] Mariotto G, Murphy S and Shvets I V 2002 *Phys. Rev.* B **66** 245426
Shvets I V, Mariotto G, Jordan K, Berdunov N, Kantor R and Murphy S 2004 *Phys. Rev.* B **70** 155406
[24] Moews A, Kurmaev E Z, Finkelstein L D, Galakhov A V, Gota S, Gautier-Soyer M, Rueff J P and Hague C F 2003 *J. Phys.: Condens. Matter* **15** 2017
[25] Cai Y Q, Nakatsuji K, Ohno S, Iimori T, Yamada M and Komori F 2002 *Surf. Rev. Lett.* **9** 907
[26] Schrupp D, Sing M, Tsunekawa M, Fujiwara H, Kasai S, Sekiyama A, Suga S, Muro T, Braber V A M and Claessen R 2004 *Preprint* cond-mat/0405623
[27] Toyoda T, Sasaki S and Tanaka M 1999 *Am. Mineral.* **84** 294
[28] Garcia J, Subias G, Proietti M G, Renevier H, Joly Y, Hodeau J L, Blasco J, Sanchez M C and Berar J F 2000 *Phys. Rev. Lett.* **85** 578
Garcia J, Subias G, Proietti M G, Blasco J, Renevier H, Hodeau J L and Joly Y 2001 *Phys. Rev.* B **63** 054110
Subias G, Garcia J, Blasco J, Proietti M G, Renevier H and Sanchez M C 2004 *Phys. Rev. Lett.* **93** 156408
[29] Attfield J P 1990 *Nature* **343** 46
[30] Wikinson A P and Cheetham A K 1991 *Acta Crystallogr.* B **47** 155
[31] Warner J K, Cheetham A K, Cox D E and Von Dreele R B 1992 *J. Am. Chem. Soc.* **114** 6074
[32] Kobayashi K, Kawata H and Mori K 1998 *J. Synchrotron Radiat.* **5** 972
[33] Larson A C and Von Dreele R B 1999 *Los Alamos National Laboratory Report* No. LAUR 86-748
[34] Lorimer J, Bernard F, Niepce J-C, Guigue-Millot N, Isnard O and Berar J-F 2003 *J. Appl. Crystallogr.* **36** 301
[35] Toyoda T, Sasaki S and Tanaka M 1997 *Japan. J. Appl. Phys.* **36** 2247